Available online at www.sciencedirect.com

ScienceDirect

Journal of Magnesium and Alloys 11 (2023) 4498–4512

www.elsevier.com/locate/jma

Full Length Article

Dissociation of edge and screw pyramidal I and II dislocations in magnesium

Yang Yang[a], Fei Liu[b], Kefan Chen[a], Boyu Liu[b], Zhiwei Shan[b], Bin Li[a,*]

[a] *Department of Chemical and Materials Engineering, University of Nevada, Reno, NV 89557, USA*

[b] *Center for Advancing Materials Performance From The Nanoscale (CAMP-Nano) and Hysitron Applied Research Center in China (HARCC), State Key Laboratory for Mechanical Behavior of Materials, Xi'an Jiaotong University, Xi'an 710049, PR China*

Received 13 November 2022; received in revised form 27 May 2023; accepted 23 June 2023

Available online 4 August 2023

Abstract

Pyramidal dislocations in magnesium (Mg) and other hexagonal close-packed metals play an important role in accommodating plastic strains along the *c*-axis. Bulk single crystal Mg only presents very limited plasticity in *c*-axis compression, and this behavior was attributed to out-of-plane dissociation of pyramidal dislocations onto the basal plane and resulted in an immobile dislocation configuration. In contrast, other simulations and experiments reported in-plane dissociation of pyramidal dislocations on their slip planes. Thus, the core structure and mode of dissociation of pyramidal dislocations are still not well understood. To better understand the dissociation behavior of pyramidal dislocations in Mg at room temperature, in this work, atomistic simulations were conducted to investigate four types of pyramidal dislocations at 300 K: edge and screw Py-I on $\{10\bar{1}1\}$, edge and screw Py-II on $\{11\bar{2}2\}$ by using a modified embedded atom method (MEAM) potential for Mg and anisotropic elasticity dislocation model. The results show that when energy minimization was performed before relaxation, in-plane dissociation of edge dislocations on respective pyramidal plane could be obtained at room temperature for all four types of dislocation. Without energy minimization, the edge dislocations dissociated out-of-plane onto the basal plane. Calculations of potential energy and hydrostatic stress of individual atoms at the edge dislocation core show that the extraordinarily high energy and atomic stresses in the as-constructed dislocation structures caused the out-of-plane dissociation onto the basal plane. The core structures of all four types of pyramidal dislocation after in-plane dissociation were analyzed by computing the distribution of the Burgers vector.

Keywords: Magnesium; Pyramidal dislocations; Atomistic simulations.

1. Introduction

Magnesium (Mg), as the lightest structural metal with a low density of 1.74 g/cm^3, is very attractive for engineering applications for improved energy efficiency. In recent years, Mg and its alloys have been studied extensively, especially in terms of mechanical properties. One of the major technical hurdles that prevents Mg alloys from widespread structural applications is their relatively low room temperature ductility [1–8]. It has been observed that, when a bulk Mg single crystal is compressed along the *c*-axis, the strain to failure is typically only a few percent [9,10]. Similar behavior has also been observed in compression of highly textured, wrought polycrystalline Mg samples, for example, along the normal direction of a rolled sheet or plate [11–15]. The mechanical behavior of Mg is inherently related to its low symmetry hexagonal close-packed (HCP) crystal structure. It is generally believed that the critical resolved shear stress (τ_{CRSS}) for different slip systems, i.e. (0002) basal, $\{1\bar{1}00\}$ prismatic, $\{10\bar{1}1\}$ (Py-I) and $\{11\bar{2}2\}$ (Py-II) pyramidal, varies significantly. The basal slip has the lowest τ_{CRSS} which is one to two orders of magnitude lower than that of the prismatic and pyramidal slip [16–23]. Thus, during plastic deformation, basal slip occurs predominantly [24–26]. But the basal slip only provides two independent slip systems. Therefore, the lack of

* Corresponding author.
E-mail address: binl@unr.edu (B. Li).

https://doi.org/10.1016/j.jma.2023.06.013

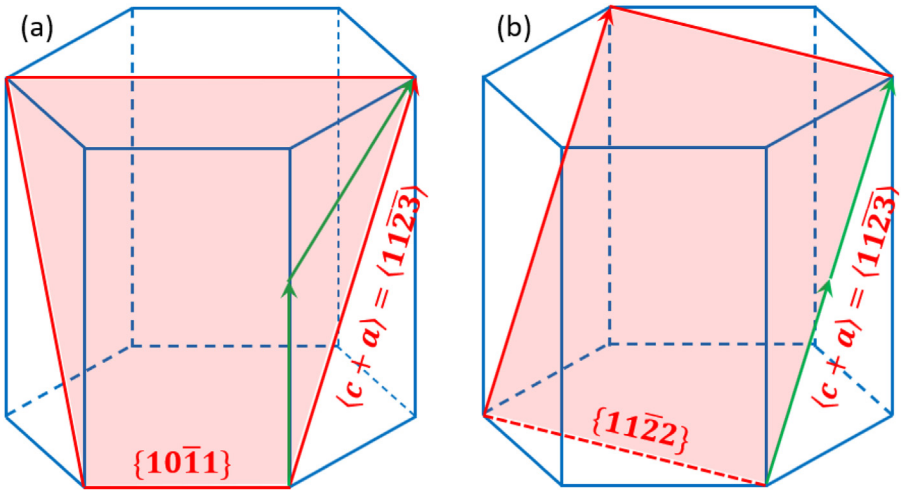

Fig. 1. (a) Py-I $\langle c+a\rangle$ dislocation on the $\{10\bar{1}1\}$ plane (the shaded). The two green arrows represent the partial dislocations as a result of dissociation of the Py-I dislocation [29]. (b) Py-II $\langle c+a\rangle$ dislocation on the $\{11\bar{2}2\}$ plane (the shaded). The large Burgers vector dissociates into two equal partial dislocations indicated by the two green arrows [30].

sufficient easy slip systems gives rise to the low room temperature ductility. However, Bhattacharya [27], Bhattacharya and Niewczas [28] showed in experiments that high purity Mg (~99.999%) single crystals presented superior ductility over a wide range of temperatures (from 4.2 K to 300 K) when deformed along different directions, contrary to the well accepted notion that Mg has low ductility at room temperature. These contrasting results in the literature raise an interesting question as to whether Mg is intrinsically brittle or not.

Activation of pyramidal dislocations is crucial to the ductility of Mg. These dislocations are necessary for accommodating the strains along the *c*-axis, because basal and prismatic dislocations cannot. Fig. 1a and b schematically show the two pyramidal slip systems, i.e., Py-I and Py-II in HCP metals. Possible dissociation of these dislocations is schematically shown by the green arrows which represent the Burgers vectors of partial dislocations [29,30]. Due to the significance of these dislocations for the plasticity of Mg, extensive experimental and simulation investigations have been conducted, in order to understand the origin of low ductility of Mg and its connection to the dissociation and motion of pyramidal dislocations. Wu and Curtin [31] conducted atomistic simulations of dissociation of an edge Py-II dislocation. They suggested that Py-II dislocations with a Burgers vector of $\frac{1}{3}\langle 11\bar{2}\bar{3}\rangle_{\{11\bar{2}2\}}$ tended to dissociate onto the basal plane, and this out-of-plane dissociation could be facilitated thermally and created an immobile configuration: two Frank partials on the basal plane connected by an I_1 basal stacking fault. This mode of dissociation was deemed the root cause of the low ductility of Mg. Similar out-of-plane dissociation was also obtained for a mixed Py-I dislocations [32]. Prior to these simulation works, pyramidal dislocations and their dissociations were studied by other researchers in simulations [33–40], but different dissociation modes were reported. Minonishi et al. [36] simulated the core structure of a $\frac{1}{3}\langle 11\bar{2}\bar{3}\rangle_{\{11\bar{2}2\}}$ edge dislocation in HCP metals using a truncated Lennard-Jones pair potential. After dissociation, structural units close to $\{11\bar{2}2\}$ and $\{11\bar{2}1\}$ twins were observed near the dislocation core. Minonishi et al. [35] also simulated the motion of $\frac{1}{3}\langle 11\bar{2}\bar{3}\rangle$ screw dislocations under various loading conditions and found that irrespective of the core structure, the pyramidal dislocations were mobile on either $\{11\bar{2}2\}$ or $\{10\bar{1}1\}$ plane. In-plane and out-of-plane dissociation of a mixed Py-I dislocation parallel to the $[1\bar{2}10]$ were observed by Numakura et al. [33,34]. In their work, a mixed Py-I dislocation extended onto the basal plane. Non-planar dissociation of a Py-II dislocation was observed by Liang and Bacon [38] as well. Possible dissociation of pyramidal dislocations was also studied by Morris et al. [40] by calculating the generalized stacking fault energy which has been used to predict probable low energy dissociation paths. In addition to those works in which a pyramidal dislocation was constructed, activation of pyramidal slip was also investigated by deforming a perfect single crystal Mg in simulations, and indeed, pyramidal dislocations without out-of-plane dissociation were obtained but mostly on the $\{10\bar{1}1\}$ plane [29,41,22]. Non-planar glide of $\langle c+a\rangle$ screw dislocations on pyramidal planes via atomic shuffling and kink pair formation on the trailing partial was reported by Srivastava et al. [42]. Ghazisaeidi et al. [30] investigated the dissociation of a Py-II edge and screw dislocation using first principles simulation and showed that a full Py-II dislocation dissociates into two $\frac{1}{2}\langle c+a\rangle$ partials. Depending on the simulation method and interatomic potentials that were used in the simulation, discrepancies can be seen in the literature reports, and the dissociation of pyramidal dislocations remains not well understood.

Post-mortem transmission electron microscopy (TEM) was conducted by researchers to investigate pyramidal dislocation slip in HCP metals [16,43–52,35,53,54]. In these works, the morphology of pyramidal dislocations appeared to be straight lines that are parallel to the trace of the basal plane, but these dislocations did present both $\langle c\rangle$ and $\langle a\rangle$ component

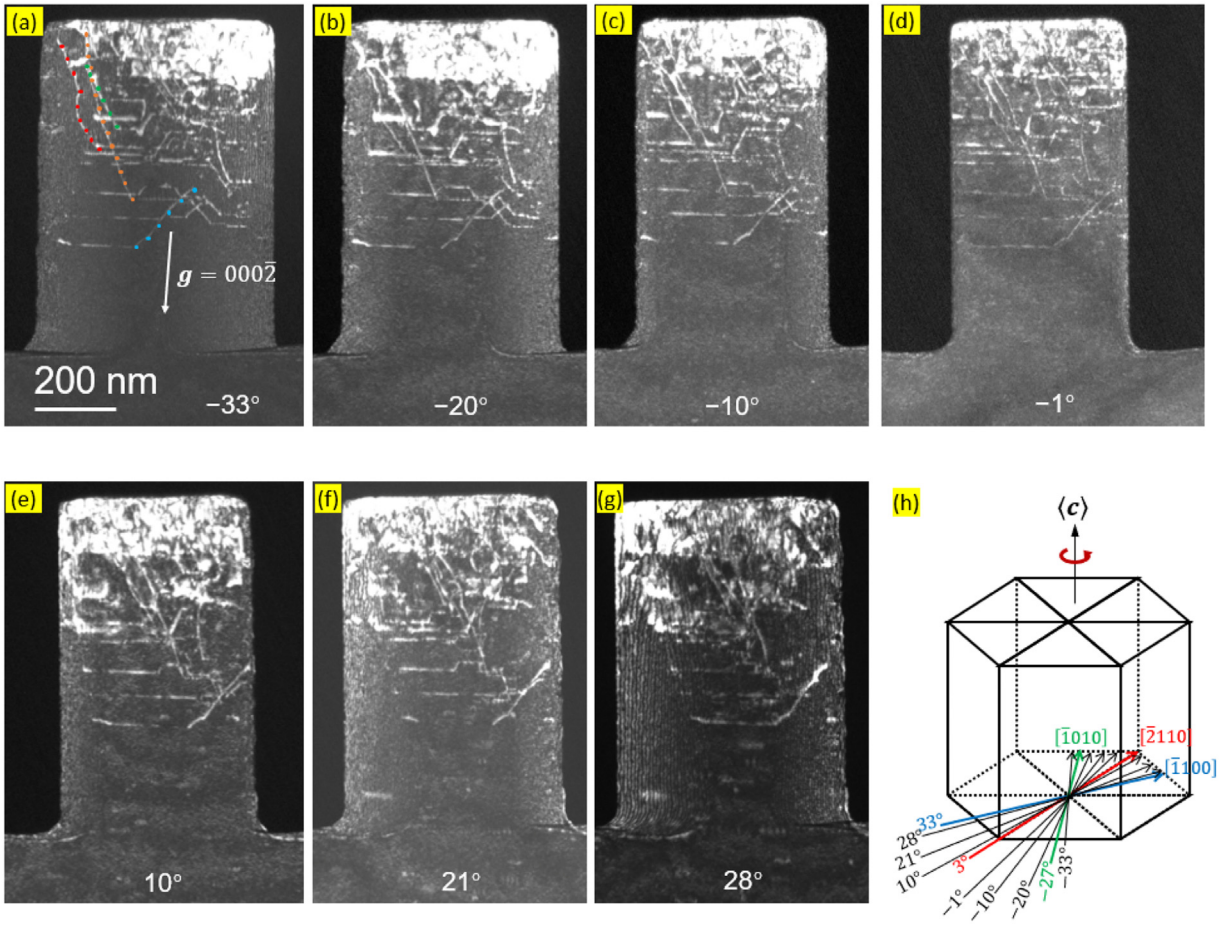

Fig. 2. Activation of pyramidal dislocations in a submicron Mg pillar after *c*-axis compression. A series of dark field TEM images (a-h) are obtained by rotating the deformed pillar around the *c*-axis. Four of the pyramidal dislocations are highlighted by red, orange, green and blue dots in (a). The electron beam direction and the angular intervals are indicated in (h). The diffraction contrast show that pyramidal dislocations are activated during deformation. The 3D reconstructed dislocation structure is provided in Supplemental Material.

in diffraction contrast analysis. It should be noted that such a morphology in TEM does not necessarily indicate dissociation of pyramidal dislocations onto the basal plane. Careful specimen tilting is needed to resolve the dislocations at different zone axes. Preferably, weak beam dark field (WBDF) imaging at different zone axes should be conducted. Most recently, Liu et al. [55] performed in-situ TEM to observe pyramidal dislocations. Both Py-I and Py-II dislocations were confirmed by using 3D tomography. Fig. 2a-g shows dark field TEM images in which a Mg single crystal was compressed on the top approximately along the *c*-axis. The images were taken by rotating the deformed Mg pillar and then imaging at various angles (Fig. 2h). Note that the reflection $\boldsymbol{g} = 000\bar{2}$ was used to image the dislocations, hence, the visible dislocations have a strong ⟨*c*⟩ component. Thus, these dislocations are neither basal nor prismatic, but are pyramidal dislocations. The 3D reconstructed dislocation structure is provided in Supplemental Material 1. These in-situ TEM observations indicate that pyramidal dislocations are stable and mobile, although the dissociated core structure is hard to resolve in TEM.

Despite extensive research on pyramidal dislocations in HCP metals over the past few decades, dislocation core structure and mode of dissociation are still not well understood. Additionally, how an edge Py-I dislocation in Mg dissociates has not been reported. This motivates the present work to investigate and understand the core structure and dissociation behavior of edge and screw Py-I and Py-II dislocations in Mg at room temperature, by using atomistic simulations. In particular, in-plane and out-of-plane dissociation of pyramidal dislocations are carefully examined, and the reason behind is analyzed and discussed. The results obtained provide new insight on the nature of pyramidal slip in HCP metals.

2. Simulation method

Modified embedded atom method (MEAM) [56,57] potential for Mg was used in this work. This MEAM potential was developed by Wu et al. [58]. The software package Atomsk [59] was used for constructing all the pyramidal dislocations. Four types of pyramidal dislocation were considered: (1) Py-I edge; (2) Py-II edge; (3) Py-I screw; and (4) Py-II screw. In our simulations, dislocations were introduced into a single crystal Mg by using anisotropic elasticity model so that our results can be compared with the results reported in the

literature. The classical sextic anisotropic elasticity theory of straight dislocations was developed by Eshelby et al. [60] and extended by Foreman [61] to include anisotropy in energy calculations. The elastic constants for creating a dislocation in an anisotropic material were obtained from Ref. [31].

In our simulations, firstly we constructed a perfect HCP Mg single crystal with dimensions of 20 nm × 20 nm × 20 nm, and then a straight dislocation was introduced into the center of the Mg matrix by using Atomsk. We noted that for pyramidal dislocations with very complex core structures, the position of the initial dislocation core significantly affected the output configuration. In our construction, we searched for a relatively low energy dislocation core while the coordinates of the core were varied by fine-tuning the core position in the simulation cell. Secondly, in order to compute the per-atom Nye tensor [62] which is calculated by comparing the reference lattice of a perfect HCP crystal to the dislocated lattice, the total atoms of the reference lattice and the dislocated lattice should be equal. So, the edge dislocations were constructed by using the method without changing the total number of particles. For screw dislocations, this is not an issue because there is no extra half-atomic plane, unlike edge dislocations.

The above method worked well for creating an edge Py-II dislocation. After energy minimization and relaxation, a stable Py-II edge dislocation was obtained. But unexpectedly, it was very difficult to obtain an edge Py-I dislocation by using a similar method. A possible reason might be that, along the line direction of the edge Py-I dislocation, periodicity is very poorly defined. To overcome this difficulty, instead of directly creating an edge Py-I dislocation in the single crystal Mg, a very large Py-I dislocation loop with a radius of 150 nm was first created on the $\{10\bar{1}1\}$ plane. Then, a small portion with dimensions of 20 nm × 20 nm × 20 nm, which contains mostly the edge part of the loop, was taken out of the large system box and used as the initial structure. Then energy minimization followed by dynamic relaxation were performed.

Large-scale atomic/molecular massively parallel simulator (LAMMPS) [63] was used for all the simulations and calculations. All the as-constructed Py-I and Py-II dislocations were first energy-minimized. This step turned out to be crucially important to obtain a stable pyramidal dislocation. After energy minimization, the system was fully relaxed. This conspicuous difference between the results with and without energy minimization is presented in the following. The temperature of our simulations was maintained at 300 K by applying the Nose-Hoover thermostat [64,65]. Free surfaces were applied to all three dimensions. Conjugate gradient (CG) algorithm was used for energy minimization, the stopping tolerance for energy was 10^{-20}, and the stopping tolerance for force was 10^{-20} eV/Å, and the maximum iteration number was set at 100,000. Typically, the system took about 1,000∼2,000 steps to reach an energy minimum, depending on the system size. For dynamic relaxation, the systems were run for 100 ps (the time step size was 1.0 fs). The visualization package Ovito [66] was used to analyze the simulation results. Common neighbor analysis (CNA) [67] was used to distinguish the crystal structures and lattice defects. The atomic stress and potential energy per atom were computed during MD simulations by LAMMPS. The Nye tensor [68], which describes the degree of lattice distortion at the dislocation core were calculated by using Atomsk.

3. Simulation results

3.1. Dissociation of pyramidal edge dislocations

First, we present the simulation results of how a constructed Py-II edge dislocation dissociates. The structure of the as-constructed Py-II edge dislocation is displayed in Fig. 3a. Only a thin slice (1.0 nm thick) is shown along the viewing direction, $\langle 1\bar{1}00\rangle$, which is the direction of the edge dislocation line. In the CNA, atoms in red are in the HCP lattice, and atoms in yellow represent the dislocation core with a large lattice distortion. Fig. 3b shows that, after energy minimization followed by relaxation, the Py-II edge dislocation dissociates into two edge partial dislocations connected by a stacking fault (SF). Notably, the plane of SF remains on the Py-II, $\{11\bar{2}2\}$ plane, not the basal plane. The SF has a width of roughly 1.8 nm. The trace of the slip plane $\{11\bar{2}2\}$ is denoted by the dashed black line. Burgers circuit analysis indicates that Py-II edge dislocation dissociates into two identical partials: $\frac{1}{3}[11\bar{2}\bar{3}] \rightarrow \frac{1}{2}\cdot\frac{1}{3}[11\bar{2}\bar{3}] + \mathrm{SF} + \frac{1}{2}\cdot\frac{1}{3}[11\bar{2}\bar{3}]$. This in-plane dissociation mode was previously reported by Tang et al. [41] and Fan et al. [22,69] and Morris et al. [40].

However, in sharp contrast to Fig. 3a in which the as-constructed Py-II edge dislocation was energy minimized and then relaxed, if only relaxation was performed without the preceding step of energy minimization, the result was completely different. The result is shown in Fig. 3c. It can be seen that the as-constructed Py-II edge dislocation dissociates onto the basal plane, rather than onto the $\{11\bar{2}2\}$ plane which is the original slip plane. This scenario is somewhat similar to the "out-of-plane" dissociation of Py-II edge dislocation [31]. An I_1 SF (displayed as the green atoms) is bounded by two immobile Frank partials (displayed as yellow atoms). This configuration, which lies on the basal plane as a result of the out-of-plane dissociation, was deemed immobile and the root cause of low ductility of Mg [31].

The dissociation of a Py-I edge dislocation is similar to that of the Py-II edge dislocation. The results are shown in Fig. 4. The as-constructed Py-I edge dislocation is shown in Fig. 4a in which the dislocation line is slightly inclined with the viewing direction $\langle 2\bar{1}\bar{1}0\rangle$. Energy minimization was first performed, followed by relaxation. It is seen (Fig. 4b) that the as-constructed Py-I edge dislocation dissociated into two partial edge dislocations. Between the two partials, an SF with a width of ∼2.5 nm can be observed. The plane in which the SF lies can be identified as the $\{0\bar{1}11\}$, which is exactly the slip plane of Py-I dislocations. Burgers circuit analysis shows that the leading partial has a Burgers vector of $\frac{1}{2}\cdot\frac{1}{2}[01\bar{1}2]$ and the trailing partial has a Burgers vector along the $\frac{1}{2}\cdot\frac{1}{2}[01\bar{1}2]+\frac{1}{2}\cdot\frac{1}{3}[2\bar{1}\bar{1}0]$, i.e., the trailing partial has a half

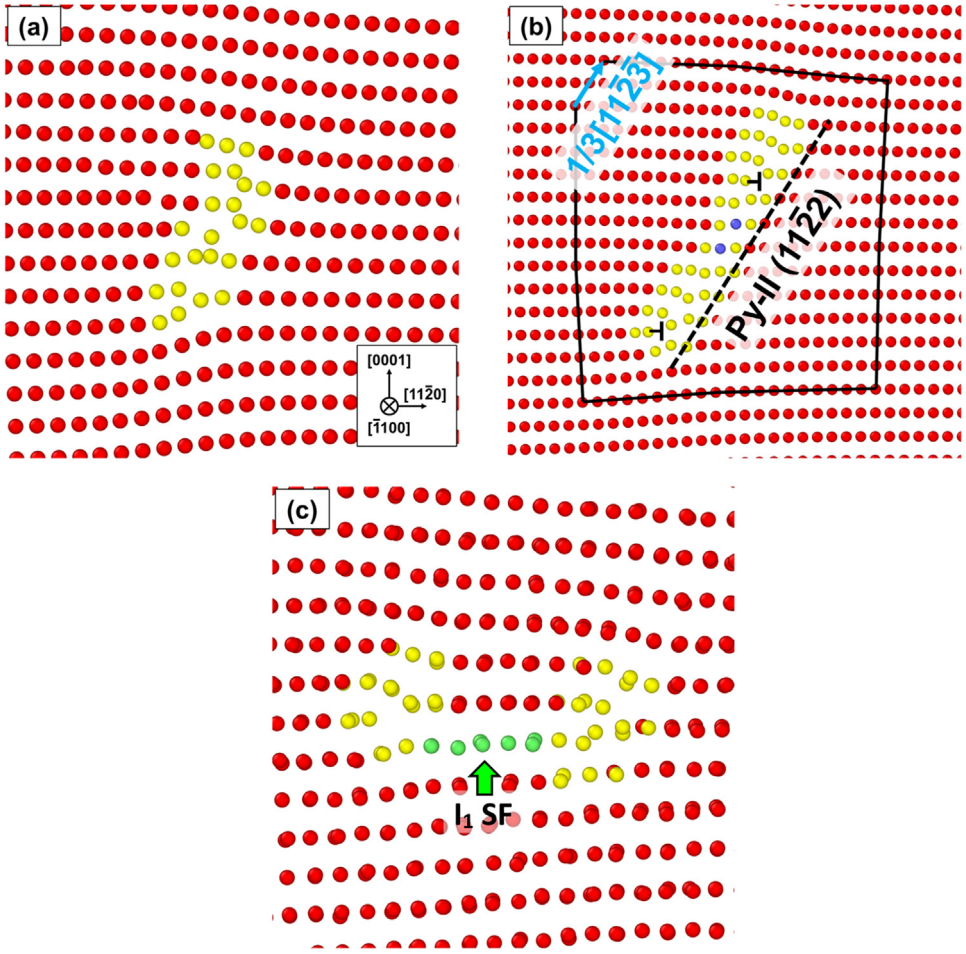

Fig. 3. (a) The core structure of the as-constructed ⟨c + a⟩ Py-II edge dislocation before energy minimization. Atoms are colored according to the local crystal structures identified with common neighbor analysis (CNA). The red atoms are in hcp lattice, and the yellow atoms are located at the dislocation core. (b) After energy minimization and relaxation, the dislocation dissociates into two partials connected by a stacking fault (SF) on {11$\bar{2}$2}. The SF width is about 1.8 nm. The dashed line indicates the trace of the slip plane, {11$\bar{2}$2}. (c) If the as constructed structure in (a) is directly relaxed without energy minimization, the ⟨$c + a$⟩ dislocation dissociates onto the basal plane, and an I_1 SF (the green atoms) is created on the basal plane.

⟨a⟩ component $\frac{1}{2} \cdot \frac{1}{3}[2\bar{1}\bar{1}0]$ [29]. A Burgers circuit analysis is provided in Fig. S1 of Supplemental Material 2. Along the viewing direction of Fig. 4b, the half ⟨a⟩ component cannot be seen because this component is exactly parallel to the viewing direction. However, if only relaxation was performed without energy minimization, the as-constructed Py-I dislocation dissociated into two immobile dislocations on the basal that are connected by an I_1 SF (displayed in green) in between. The final structure of this dissociation of the Py-I edge dislocation is shown in Fig. 4c.

3.2. Dissociation of pyramidal screw dislocations

Unlike the edge dislocations, dissociation of the as-constructed screw dislocations, irrespective of Py-I or Py-II, is always in-plane with or without energy minimization. All the as-constructed screw dislocations can be relaxed and then dissociated into an in-plane structure on their respective slip plane, and no out-of-plane dissociation onto the basal plane was observed.

The core structure of the initial, as-constructed Py-II screw dislocation is shown in Fig .5a, in which the viewing direction is tilted to the [11$\bar{2}$0] to better reveal the structure of the dissociated dislocation. The atoms at the core are displayed in yellow. After relaxation, the screw dislocation dissociated into two slightly separated partial dislocations (Fig. 5b). The split distance between the partials is ∼1.0 nm. The extended core of the dissociated screw dislocation can be better viewed when the CNA is turned off, as shown in Fig. 5c. In this plot, the original color pattern of the single crystal is shown, in which the basal stacking sequence …*ABABAB*… is displayed alternately in green and in yellow. The solid blue and dashed red lines clearly reveal the spiral structure of the screw dislocation core. The components of the Burgers vector along the c-axis are composed of splitting of every two basal planes, which exactly equals a full ⟨c⟩ component of the ⟨$c + a$⟩ dislocation.

The dissociation of the as-constructed Py-I screw dislocation is shown in Fig. 6a and b. In these plots, the viewing direction is tilted to the [11$\bar{2}$3], i.e., along the line vector of the

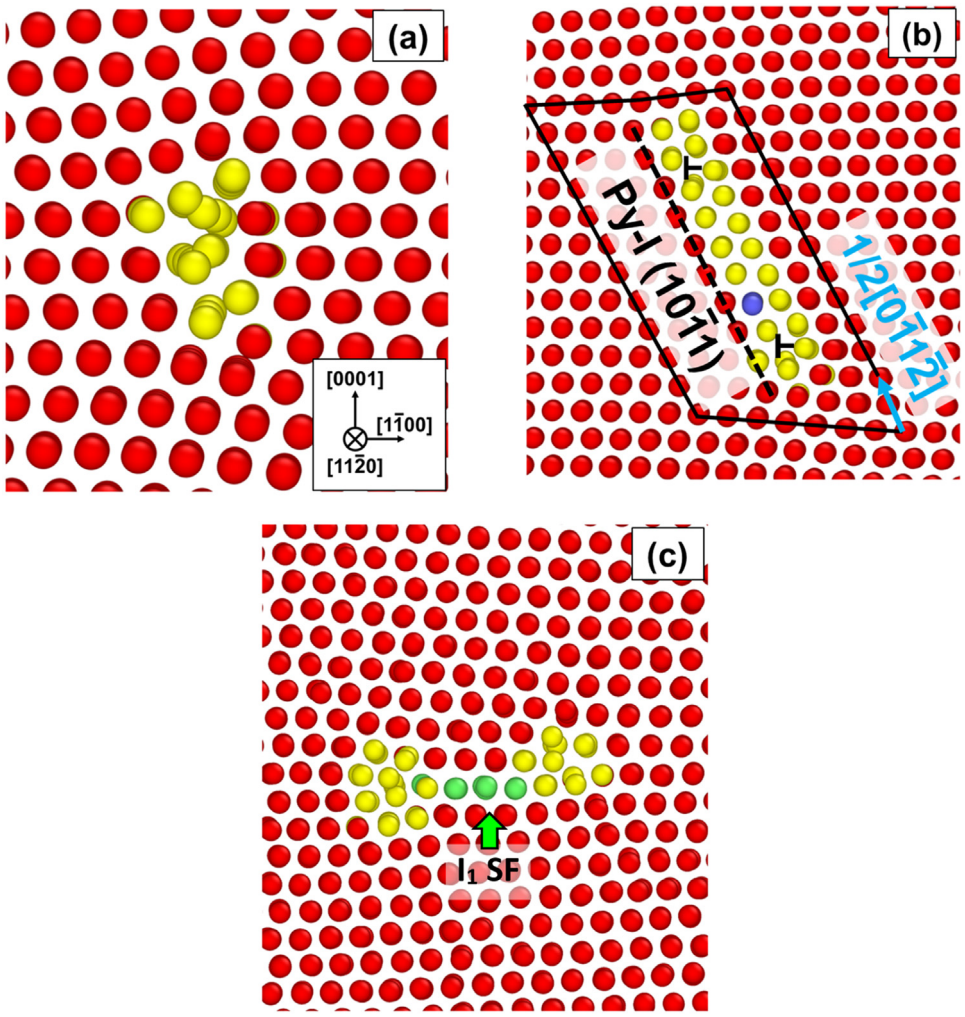

Fig. 4. (a) The core structure of an as-constructed Py-I edge dislocation before energy minimization. The yellow atoms are at the dislocation core. (b) After energy minimization and relaxation, the dislocation dissociates into two partials connected by a stacking fault (~2.5 nm) on the {10$\bar{1}$1} plane. The trace of the slip plane is indicated by the dashed black line. (c) If the as-constructed dislocation is relaxed without energy minimization, the dislocation dissociates onto the basal plane and an I_1 SF is created on the basal plane.

screw dislocation. After relaxation, the atoms at the dislocation core are spread on the {0$\bar{1}$11} slip plane (denoted by the black dashed line in Fig. 6b), rather than on the basal plane. When the viewing direction is tilted to the [01$\bar{1}$0] (Fig. 6c), the spiral structure of the screw dislocation can be well resolved, as denoted by the solid blue and dashed red lines. The core structure is similar to that of the Py-II screw dislocation (Fig. 5c)

In summary of the simulation results, for the as-constructed edge dislocations, both Py-I and Py-II, an additional step, i.e., energy minimization before relaxation is crucially important to obtain a stable core structure of in-plane dissociation on their individual slip planes. For the as-constructed screw dislocations, both Py-I and Py-II, relaxation can be performed in the simulation without the need of energy minimization, and the as-constructed screw dislocations stably dissociate onto their individual slip planes. Table 1 summarizes the dissociation behavior obtained in our simulations.

Table 1
Dissociation behavior of pyramidal dislocations with and without energy minimization before relaxation

	With energy minimization	Without energy minimization
Py-I edge	In-plane	Out-of-plane
Py-I screw	In-plane	In-plane
Py-II edge	In-plane	Out-of-plane
Py-II screw	In-plane	In-plane

4. Analysis and discussion

The simulation results obtained in this work are consistent with those in the literature in which in-plane dissociated, mobile Py-I and Py-II dislocations were obtained when a Mg single crystal was deformed and no pre-constructed pyramidal dislocations were introduced before deformation [29,41,22]. The fact that no energy minimization is needed for the as-constructed screw Py-I and Py-II dislocations and direct re-

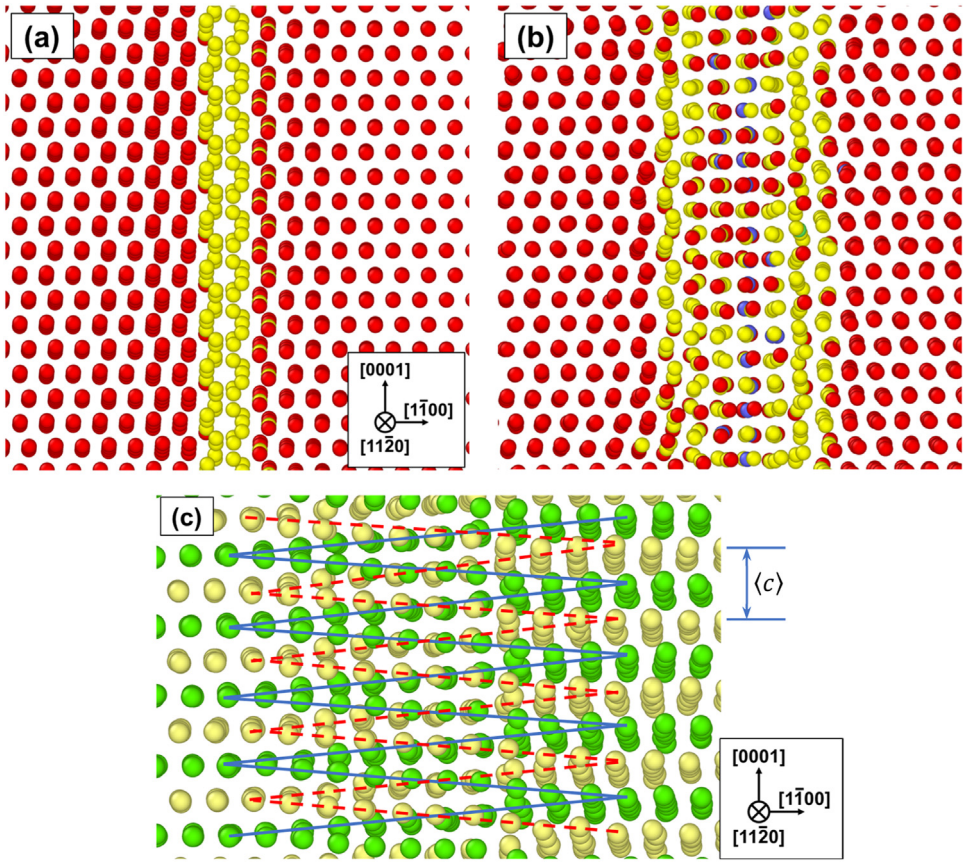

Fig. 5. (a) The core structure of the initial, as-constructed Py-II screw dislocation. The viewing direction is tilted to the [11$\bar{2}$0]. (b) After relaxation, the dislocation dissociates into two partials with a narrow stacking fault (∼1.0 nm) in between. (c) The CNA is turned off. The basal planes are now colored alternately in green and yellow for a better revelation of the dislocation core. The solid blue and the dashed red lines denote the "screw" structure along the dislocation line.

laxation generates in-plane dissociation of these dislocations (Figs. 5-6), whereas for the as-constructed edge Py-I and Py-II dislocations, energy minimization is needed before dynamic relaxation (Figs. 3-4), indicates the importance of energy minimization in the atomistic simulations where complex structures are introduced are used. In our cases of out-of-plane dissociations of the edge Py-I and Py-II dislocations onto the basal plane at 300 K, such a dissociation behavior is likely to be caused by the extremely high energies or stresses in the as-constructed configurations.

For comparison, we also tested the EAM potential developed by Liu et al. [70] by using similar technique. These results are shown in Supplemental Material 2. The EAM potential is able to describe in-plane dissociation of edge and screw Py-I dislocations (Fig. S2-S3), but not Py-II dislocations. Unexpected structures were obtained (Fig. S4-S5). These differences indicate that the MEAM describes better the dissociation behavior of pyramidal dislocations in Mg than does the EAM which does not include angular bonding in its formulism. Additionally, the MEAM potential predicts the stacking fault energy with a better accuracy than does the EAM. These factors may contribute to the observed differences.

In the following, we quantitatively compute and compare the potential energy, hydrostatic stresses of individual atoms at the dislocation core before and after energy minimization and relaxation.

4.1. Analysis of the potential energy at the dislocation core

The potential distribution of the as-constructed Py-II edge dislocation is shown in Fig. 7a. This distribution is plotted over a region of ∼5 nm × 5 nm and 1 nm thick that contains the dislocation core in the center, with the dislocation line along the thickness direction (see Fig. 3a). For clarity, the atoms in the selected region are displayed below the energy plot with those atoms at the dislocation core displayed in dark green and the other atoms in pink. The potential energy of each atom of the as-constructed structure is computed and plotted. It is seen that the highest potential energy of the selected atoms is −0.36 eV/atom. After energy minimization followed by relaxation, the highest potential energy drops to −1.27 eV/atom (Fig. 7b), and the two energy peaks represent the core of the two partial dislocations lying on the {11$\bar{2}$2} plane after stable dissociation. It is worth noting that, if no energy minimization and only relaxation was applied, the Py-II edge dislocation dissociates onto the basal plane (see Fig. 3c), but the minimum energy is similar to that of the structure with energy minimization.

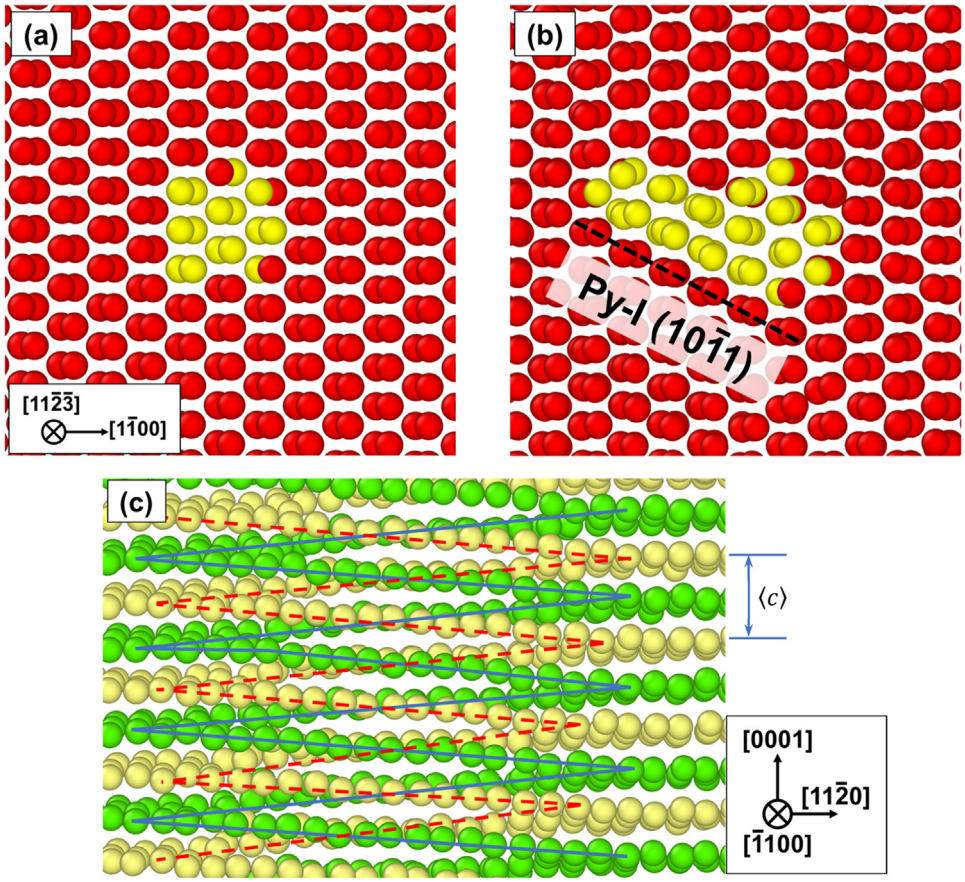

Fig. 6. (a) The core structure of an as-constructed ⟨$c + a$⟩ Py-I screw dislocation before relaxation. (b) After relaxation, the dislocation slightly dissociates into two partials which has an SF width about 1.8 nm. The dashed line indicates the slip plane, {10$\bar{1}$1}. (c) The basal planes are colored alternately in green and yellow for a better revelation of the relaxed core structure of the screw dislocation. The "screw" structure can be clearly seen.

Different from the edge Py-II dislocation which has a very high initial potential energy (Fig. 7a), the as-constructed screw Py-II dislocation has a much lower potential energy, as shown in Fig. 7c. Only the energy of each atom in a selected region ($5 \times 5 \times 1$ nm^3) is plotted. The potential energy is plotted along the dislocation line (the dark green atoms) direction. The maximum potential energy of the as-constructed screw dislocation is −0.95 eV/atom, which is nearly three times lower if compared to −0.36 eV/atom of the as-constructed edge Py-II dislocation (Fig. 7a). After relaxation without energy minimization, the initial Py-II screw dissociates onto the Py-II slip plane rather than the basal plane, and the maximum potential energy of the relaxed structure drops to −1.30 eV/atom (Fig. 7d).

A salient contrast is seen in the as-constructed Py-I edge dislocation, as shown in Fig. 8a. Before energy minimization, the maximum potential energy of the as-constructed Py-I edge dislocation is 5.48 eV/atom, which is extraordinarily high. Such a high potential energy indicates that there are atom pairs with very small separation in the as-constructed Py-I edge dislocation, and with very strong repulsive forces between them. After energy minimization followed by subsequent relaxation, the maximum potential energy drops to −1.35 eV/atom, and this value is comparable to the minimum energies in the cases of stable dissociation of Py-II edge (Fig. 7b) and Py-II screw (Fig. 7d). The high energy peak splits into two short peaks which correspond to the two partial dislocations on the {0$\bar{1}$11} plane (se Fig. 4b).

As shown in Fig. 4c, if the as-constructed Py-I edge dislocation is only relaxed without the preceding energy minimization, the edge dislocation dissociates into partial dislocations that lie on the basal plane, most likely due to the unusually high potential energy of the atoms along the constructed dislocation line. Again, this is not seen for the as-constructed Py-I screw dislocation (Fig. 8c). The as-constructed dislocation has the highest potential energy of −0.68 eV/atom, whereas the maximum energy after relaxation drops to −1.26 eV/atom (Fig. 8d).

From our results, for both Py-I and Py-II, the initial, as-constructed edge dislocations always have a significantly higher potential energy than screw dislocations. The high potential energy of edge dislocations offers a clue why the as-constructed edge dislocations tend to dissociate onto the basal plane when no energy minimization is performed before relaxation. As seen in Fig. 7-8, without minimization, the initial potential energy of the as-constructed edge dislocation is so high that the system is relaxed in a chaotic fashion to the low energy configurations on the basal plane, i.e., out-of-

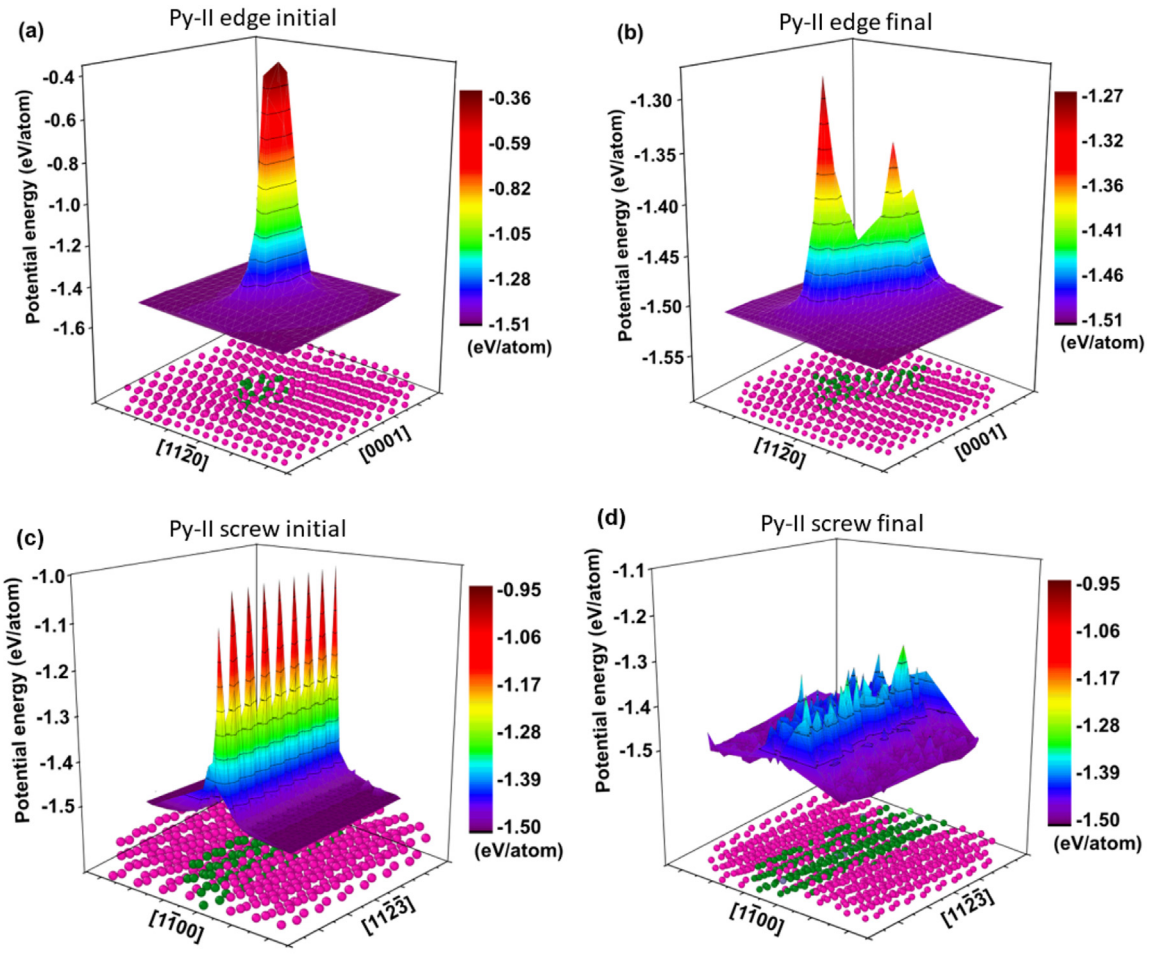

Fig. 7. (a) The potential energy distribution of the as-constructed Py-II edge dislocation. (b) The potential energy distribution of the energy minimized and relaxed dislocation. Note that the maximum potential energy of the initial structure is −0.36 eV/atom, whereas the maximum value of the energy minimized and relaxed structure is −1.27 eV/atom. The dark green atoms represent the dislocation core. (c) The potential energy distribution of the as-constructed Py-II screw. (d) The potential energy distribution of the relaxed Py-II screw. The maximum potential energy of the as-constructed structure is −0.95 eV/atom, whereas the maximum value of the relaxed dislocation is −1.30 eV/atom. The dark green atoms represent the dislocation core.

plane dissociation. In contrast, when energy minimization is performed, the system is relaxed along a different pathway that leads to the in-plane dissociation on the pyramidal plane. For the as-constructed screw dislocations, either Py-I or Py-II, no energy minimization is needed. With and without energy minimization, very similar in-plane dissociation can always be obtained (see Fig. S6-S7 in Supplemental Material 2), likely because the initial energy is much lower than that of the edge dislocation (Figs. 7-8).

4.2. Analysis of the hydrostatic stress at the dislocation core

To further verify that the unstable dissociation of pyramidal dislocations onto the basal plane is a result of relaxation of the extraordinarily high energy state of the as-constructed configuration, in the following, hydrostatic stresses of each atom at and near the dislocation core are computed at the initial and the final state. The hydrostatic stress is computed as: $\sigma = -(W_{xx} + W_{yy} + W_{zz})/3V$, where W_{xx}, W_{yy} and W_{zz} are the diagonal components of the per-atom stress tensor that have the units of energy, and V is atomic volume [63]. Thus, to compute the hydrostatic stress, the atomic volume V must be known. However, in atomistic simulations, atomic volume is not well defined when crystalline defects such as grain boundaries, dislocations and free surfaces are present, or when the system is strained. LAMMPS provides a method to estimate the atomic volume which is computed as the volume of a Voronoi cell enclosing an atom. The Voronoi cell contains all points closer to the atom than any other atoms.

The hydrostatic stress and its distribution of the as-constructed Py-II edge dislocation is displayed in Fig. 9a. Notably, the maximum value is as large as 27.71 GPa, which is extremely high. After energy minimization and relaxation, the Py-II dislocation dissociated onto the {11$\bar{2}$2} slip plane, and the maximum value drastically drops to 6.31 GPa (Fig. 9b), only about a quarter of that of the as-constructed dislocation. In contrast, the hydrostatic stress difference between the initial and relaxed structure is not so huge in the case of Py-II screw dislocations. As shown in Fig. 9c, the maximum value of the as-constructed Py-II screw is only 13.05 GPa. After

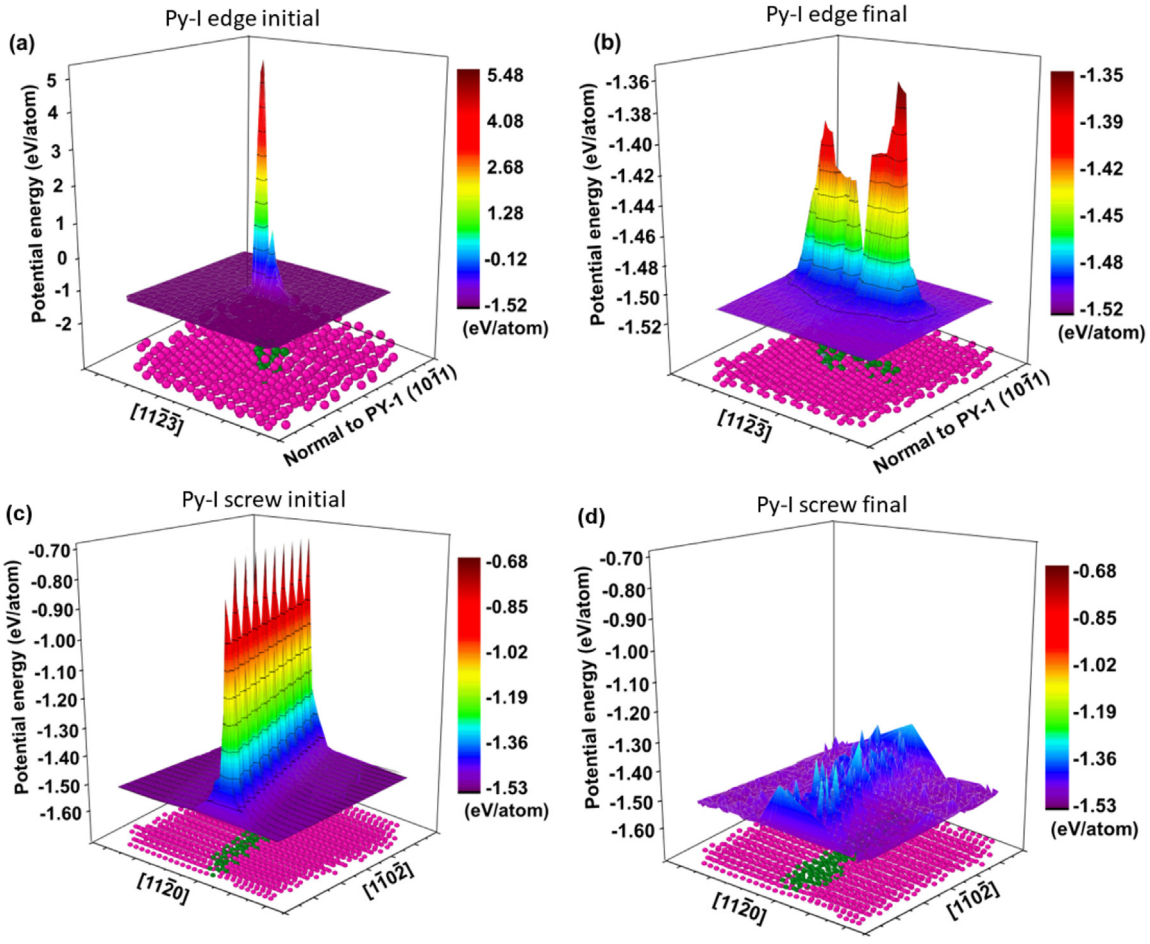

Fig. 8. (a) The potential energy distribution of the as-constructed Py-I edge dislocation. (b) The potential energy distribution after energy minimization and relaxation. The maximum potential energy of the as-constructed structure is 5.48 eV/atom, whereas the maximum value after energy minimization and relaxation is −1.35 eV/atom. The dark green atoms represent the dislocation core. (c) The potential energy distribution of the as-constructed Py-I screw. (d) The potential energy distribution of Py-I screw after relaxation. The maximum potential energy of the as-constructed screw dislocation is −0.68 eV/atom, whereas the maximum value after relaxation is −1.26 eV/atom. The dark green atoms represent the dislocation core.

relaxation without energy minimization, the Py-II screw dissociates onto the {11$\bar{2}$2} slip plane, and the maximum value drops to 4.78 GPa (Fig. 9d).

Similar to the potential energies, the hydrostatic stresses of Py-I dislocations show a huge difference between the edge and screw structure. Fig. 10a illustrates the hydrostatic stress of the as-constructed Py-I edge dislocation. It is seen that the maximum value of this initial structure is as high as 80.72 GPa, implying the presence of atom pairs in short spacings and very high repulsive forces are present. After energy minimization (Fig. 10b), the maximum value of the energy-minimized Py-I edge is only 4.85 GPa. However, for Py-I screw dislocation (Fig. 10c), the maximum value of the initial structure is only 11.03 GPa and the maximum value of the relaxed structure is 4.37 GPa (Fig. 10d). The hydrostatic stress mapping of the dissociated Py-I edge dislocation and Py-II edge dislocation is also plotted in Fig. 11a and b, respectively. In these plots, the compressive and tensile stress field of the in-plane dissociated pyramidal edge dislocations on their slip planes are mapped atom by atom. To better reveal the compressive and tensile stress field, only the range from −2 GPa to 2 GPa is shown. But actually, for the Py-I edge dislocation, the peak compressive stress is 4.61 GPa and the peak tensile stress is −3.83 GPa; for the Py-II edge dislocation, the peak compressive stress is 6.31 GPa, and the peak tensile stress is −4.76 GPa.

Conceivably, the initial edge dislocations with extraordinarily high hydrostatic stress cannot stably dissociates onto their pyramidal plane if no energy minimization is performed. If only relaxation is performed, the core structure of the edge dislocations will be relaxed into the immobile basal configurations which consist of Frank partials and an I_1 stacking fault on the basal plane, but this process is not necessarily the intrinsic behavior of the pyramidal dislocation. Thus, the high hydrostatic stresses and the high potential energies of the edge dislocations are likely the cause of the out-of-plane dissociation of pyramidal dislocations when no energy minimization is conducted for edge dislocations.

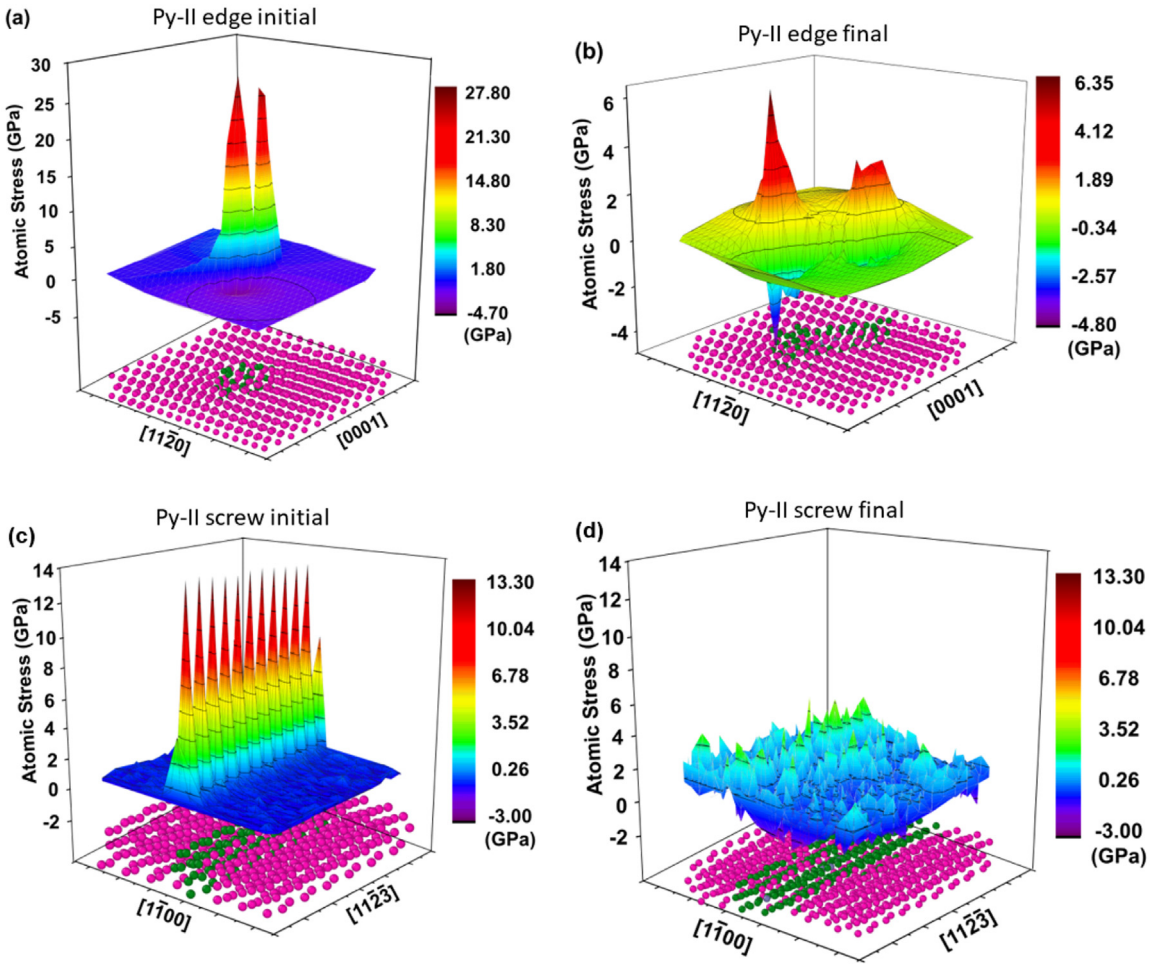

Fig. 9. (a) The atomic stress of the as-constructed Py-II edge dislocation, i.e., before energy minimization. (b) After energy-minimization and relaxation. Note that the maximum atomic stress of the initial structure is 27.71 GPa, whereas the maximum value of the energy-minimized structure is 6.31 GPa. The dark green atoms represent the dislocation core. The atomic stresses of the as-constructed structure are extremely high. (c) The atomic stress of the as-constructed Py-II screw, i.e., before energy minimization and relaxation. (d) After energy minimization and relaxation. The maximum value of the as-constructed structure is 13.05 GPa, whereas the maximum value after energy minimization and relaxation is 4.78 GPa. The Dark green atoms represent the dislocation core.

4.3. Calculation of the Nye tensor

The Nye tensor was initially used to describe the distortion of slip planes in bending of metal sheets, which can be accommodated by the presence of geometrically necessary dislocations (GNDs) [68]. Hartley and Mishin [62] demonstrated that the Nye tensor, which was initially inferred from macroscopic deformation gradient, could also be extended to describe the degree of lattice distortion near a dislocation core if the Burgers vector was treated as a sum of numerous infinitesimal Burgers vectors distributed on the slip plane. For a narrow dislocation core, most of the Burgers vectors are distributed near the core region and the majority of lattice distortion would be concentrated at the core. The reverse is true for a wide dislocation core. Using this concept, we computed the Nye tensors for the edge and screw Py-I and Py-II dislocations obtained in our simulations.

The Nye tensor α_{ij} (i represents the direction of the Burgers vector and j the direction of the dislocation line) was computed with Atomsk by comparing a perfect reference lattice with the dislocated lattice. Fig. 12a shows the distribution of α_{12} component of the Py-I edge dislocation, and Fig. 12b shows the distribution of α_{22} of the Py-I screw dislocation. Similar plots for Py-II edge and screw dislocation are shown in Fig. 12c and d, respectively. In these color plots, the atomic structure (the white spheres) of the individual dislocations is superimposed with the Nye tensor component distribution. Some interesting features can be observed from these plots. For the Py-I edge (Fig. 12a), the core mostly spreads along the normal direction of the $\{0\bar{1}11\}$ slip plane, whereas for the Py-I screw (Fig. 12b), the core also spread on the slip plane. The core of Py-II edge dislocation mostly spreads along the normal direction to the basal plane, i.e., the c-axis (Fig. 12c). But for the Py-II screw dislocation, the core mostly spread along the normal direction of the slip plane $\{11\bar{2}2\}$ (Fig. 12d).

The Nye tensor for the Py-II edge dislocation (Fig. 12c) obtained in our calculation is similar to the literature report [31]. The Nye tensor of a Py-I edge dislocation that dissociates in-plane on the $\{10\bar{1}1\}$ was not reported before, because

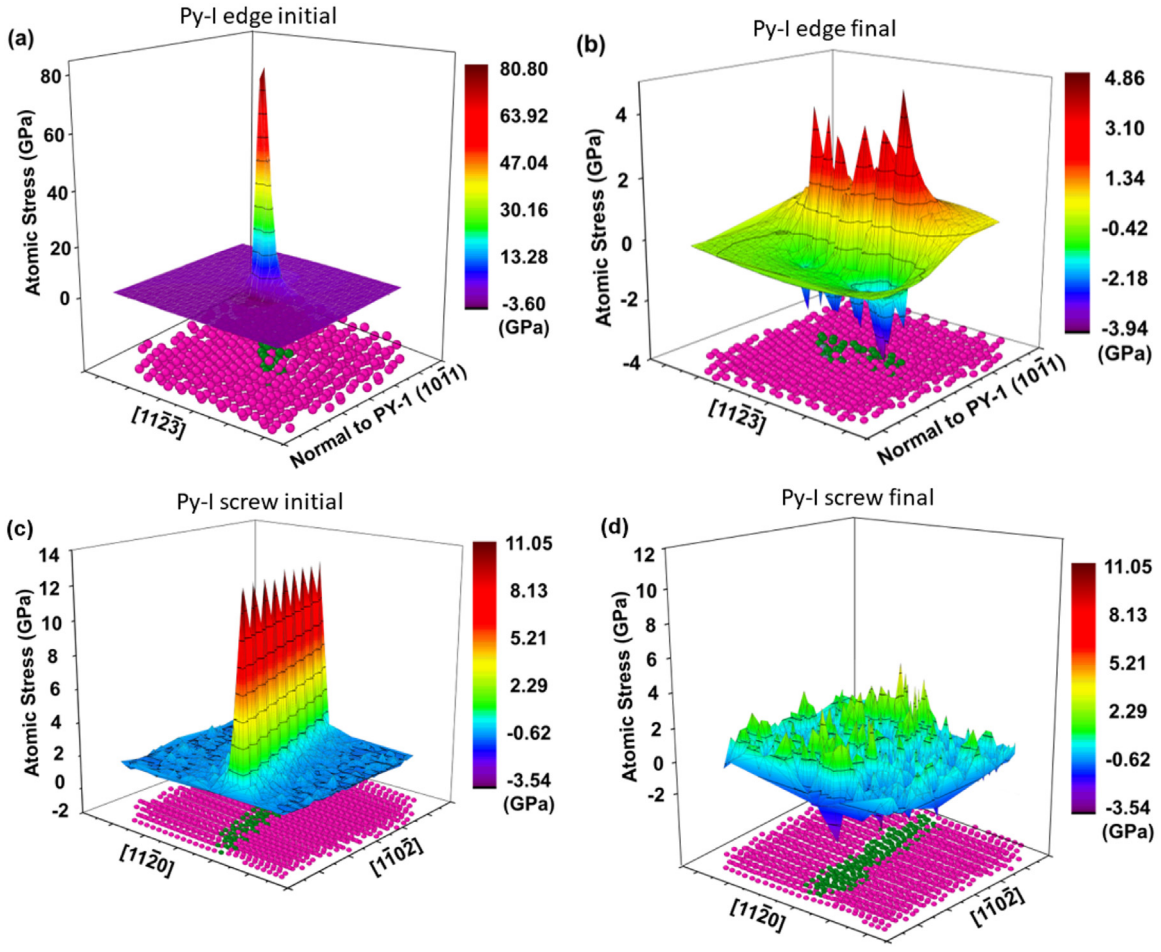

Fig. 10. (a) The atomic stress of the as-constructed Py-I edge dislocation core. (b) The atomic stresses after energy minimization and relaxation. The maximum atomic stress of the initial structure is 80.72 GPa which is extraordinarily high, whereas the maximum value of the energy-minimized and relaxed structure is only 4.85 GPa. The dark green atoms represent the dislocation core. (c) The atomic stress of the as-constructed Py-I screw. (d) The atomic stresses after relaxation (no energy minimization is needed). The maximum atomic stress of the initial structure is 11.03 GPa, whereas the maximum value of the relaxed structure is 4.37 GPa. The dark green atoms represent the dislocation core.

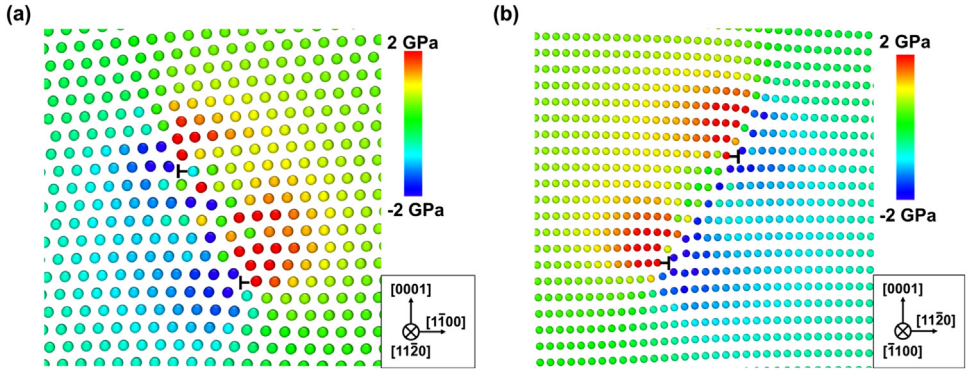

Fig. 11. (a) Mapping of the atomic stress of a dissociated Py-I edge dislocation. (b) Mapping of the atomic stress of a dissociated pyramidal II edge dislocation. For the convenience of color mapping, only the range from −2 GPa to 2 GPa is shown.

no stable configuration of dissociated Py-I edge dislocation was successfully obtained from a pre-constructed dislocation. Since the Nye tensor describes the distribution of the Burgers vector of a dislocation, the mobility of dislocation may be affected by the distribution. The motion of the dissociated edge and screw Py-I and Py-II dislocations under shear loading will be presented elsewhere.

It is seen from the present work that energy minimization should be performed when using MEAM potentials to simulate complex crystalline defects such as pyramidal disloca-

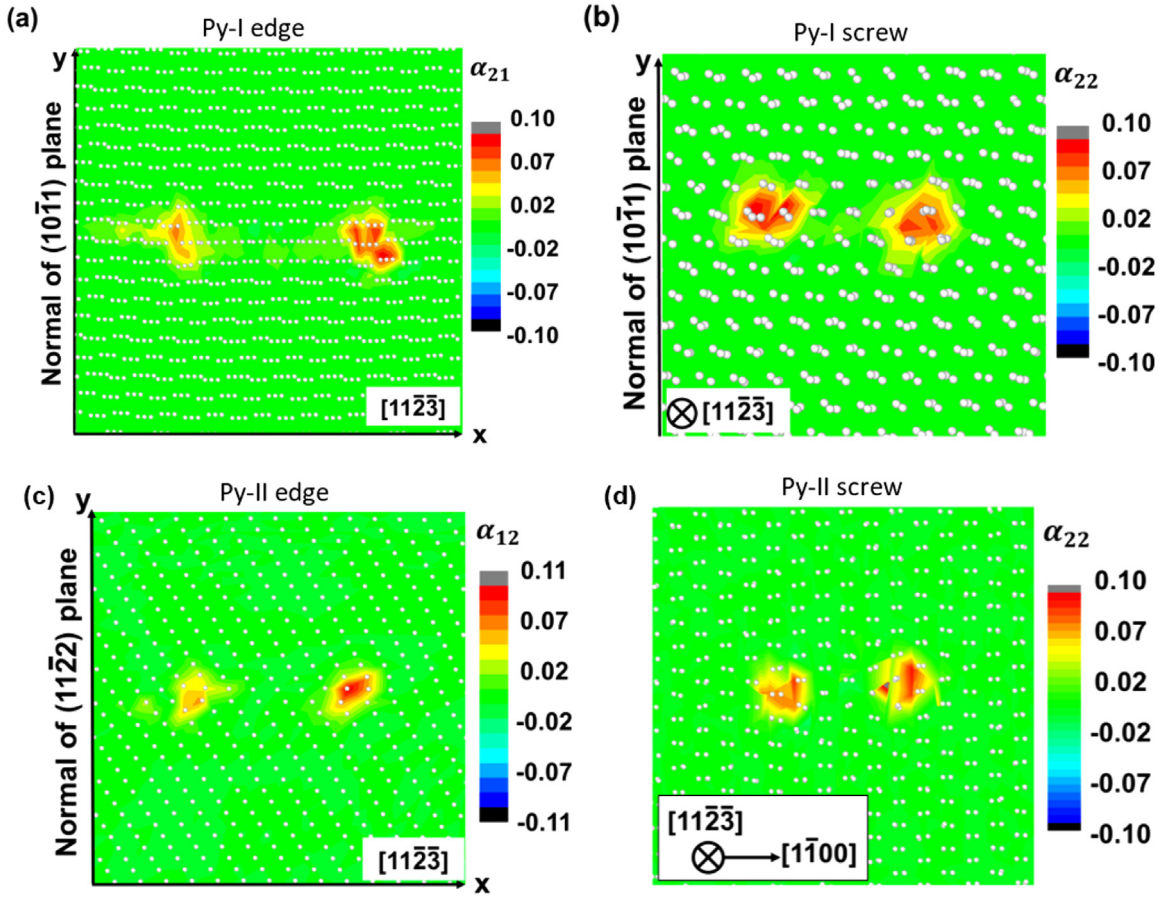

Fig. 12. (a) Distribution of α_{21} of the Py-I edge dislocation. (b) Distribution of α_{22} of the Py-I screw dislocation. (c) Distribution of α_{12} of the Nye tensor of the Py-II edge dislocation. (d) Distribution of α_{22} of the Nye tensor of the Py-II screw dislocation.

tions. Although energy minimization is often interspersed with dynamic runs, our results do show there could be a significant difference. According to LAMMPS [63], energy minimization algorithms bound the distanced atoms to move in one iteration, so that the systems with highly overlapped atoms (with high energies and forces) can be relaxed. This may explain why energy minimization should be performed before relaxation in the studies of pyramidal dislocations and other complex structures. The extraordinarily high stresses and energies of the as-constructed edge dislocations, both Py-I and Py-II, indicate the presence of such highly overlapped atoms. Thus, energy minimization is needed before relaxation such that in-plane dissociations can be obtained. In contrast, for screw pyramidal dislocations with relatively low initial potential energies and atomic stresses, they can be relaxed without energy minimization.

In actuality, when a dislocation is nucleated during plastic deformation of a crystal, irrespective of dislocation type, i.e., basal, prismatic or pyramidal, a leading partial is always nucleated first, followed by the nucleation of the trailing partial. The elastic energy of a partial dislocation is significantly lower than that of an undissociated, full dislocation. Thus, in real-life deformation, the initial energy of pyramidal dislocations, whether Py-I or Py-II, edge or screw, cannot be as high as that of the as-constructed pyramidal dislocations in atomistic simulations. Hence, in-plane dissociated, stable pyramidal dislocations are highly likely to occur during plastic deformation of Mg and other HCP metals. In small scale *c*-axis compression of Mg single crystal pillar (Fig. 1), the stress level (close to 1.0 GPa [55]) is much higher than that for bulk samples. Thus, nucleation and glide of Py-I and Py-II dislocations are highly favorable and feasible.

5. Conclusions

In this work, stable Py-I and Py-II edge and screw dislocations in pure Mg that are dissociated on respective pyramidal slip plane at 300 K are successfully obtained in atomistic simulations in which energy minimization is used prior to dynamic relaxation. The following conclusions can be reached:

(1) In atomistic simulations of complex atomic structures such as dislocation core and dissociation of pyramidal slip systems in HCP metals, energy minimization is needed before dynamic relaxation is performed. This step is crucial for achieving stable, in-plane dissociation of these dislocations.

(2) For edge dislocations, Py-I and Py-II, the as-constructed structure will dissociate into two partial dislocations on the pyramidal slip plane when energy minimization is conducted before relaxation in simulations. Without energy minimization, out-of-plane dissociation into an immobile structure on the basal plane will occur. In contrast, for screw dislocations, no energy minimization is needed, and they dissociate in-plane on the respective pyramidal slip plane after relaxation. The Py-II is dissociated into two equal partials, i.e., $\frac{1}{3}[11\bar{2}\bar{3}] \rightarrow \frac{1}{2}\cdot\frac{1}{3}[11\bar{2}\bar{3}]_{\mathrm{L}} + \mathrm{SF} + \frac{1}{2}\cdot\frac{1}{3}[11\bar{2}\bar{3}]_{\mathrm{T}}$; whereas the Py-I dissociation can be described as: $\frac{1}{3}[11\bar{2}\bar{3}] \rightarrow \frac{1}{2}\cdot\frac{1}{2}[01\bar{1}2]_{\mathrm{L}} + \mathrm{SF} + \{\frac{1}{2}\cdot\frac{1}{2}[01\bar{1}2] + \frac{1}{2}\cdot\frac{1}{3}[2\bar{1}\bar{1}0]\}_{\mathrm{T}}$.

(3) The distribution of potential energies and hydrostatic stresses of individual dislocation core structures show that the as-constructed edge dislocations contain very high potential energy and atomic stresses, which provide a clue to the out-of-plane dissociation of pyramidal dislocations.

Declaration of competing interest

The authors declare that they have no known competing financial interests or personal relationships that could have appeared to influence the work reported in this paper.

Boyu Liu and Zhiwei Shan are editorial board members for Journal of Magnesium and Alloys and were not involved in the editorial review or the decision to publish this article. All authors declare that there are no competing interests.

Acknowledgments

Bin Li gratefully thanks the support from U.S. National Science Foundation (NSF) (CMMI-2016263, 2032483). Part of this work used the Extreme Science and Engineering Discovery Environment (XSEDE) [71], which is supported by National Science Foundation grant number ACI-1548562, on Bridges Pylon at Pittsburgh Supercomputing Center through TG-MAT200001. BY Liu acknowledges the support provided by National Natural Science Foundation of China (51971168 and 52022076).

Supplementary materials

Supplementary material associated with this article can be found, in the online version, at doi:10.1016/j.jma.2023.06.013.

References

[1] J.P. Hirth, J. Lothe, T. Mura, J. Appl. Mech. 50 (1983) 476–477, doi:10.1115/1.3167075.
[2] M.K. Kulekci, Int. J. Adv. Manuf. Technol. 39 (2008) 851–865, doi:10.1007/s00170-007-1279-2.
[3] H. Friedrich, S. Schumann, J. Mater. Process. Technol. 117 (2001) 276–281, doi:10.1016/S0924-0136(01)00780-4.
[4] U.M. Chaudry, K. Hamad, J.G. Kim, J. Alloys Compd. 792 (2019) 652–664, doi:10.1016/j.jallcom.2019.04.031.
[5] Z. Wu, B. Yin, W.A. Curtin, Acta Mater. 119 (2016) 203–217, doi:10.1016/j.actamat.2016.08.002.
[6] S. Sandlöbes, S. Zaefferer, I. Schestakow, S. Yi, R. Gonzalez-Martinez, Acta Mater. 59 (2011) 429–439, doi:10.1016/j.actamat.2010.08.031.
[7] S. Sandlöbes, M. Friák, J. Neugebauer, D. Raabe, Mater. Sci. Eng. A 576 (2013) 61–68, doi:10.1016/j.msea.2013.03.006.
[8] D. Hull, D.J. Bacon, Introduction to Dislocations, Elsevier, 2011.
[9] H. Yoshinaga, R. Horiuchi, in: Trans. Jpn. Inst. Metals, 4, 1963, pp. 1–8.
[10] E.W. Kelley, W.F. Hosford Jr., Trans. Metall. Soc. AIME 242 (1968) 5–13.
[11] T. Nogaret, W.A. Curtin, J.A. Yasi, L.G. Hector, D.R. Trinkle, Acta Mater. 58 (2010) 4332–4343, doi:10.1016/j.actamat.2010.04.022.
[12] T. Obara, H. Yoshinga, S. Morozumi, Acta Metall. 21 (1973) 845–853, doi:10.1016/0001-6160(73)90141-7.
[13] K.Y. Xie, Z. Alam, A. Caffee, K.J. Hemker, Scr. Mater. 112 (2016) 75–78, doi:10.1016/j.scriptamat.2015.09.016.
[14] H. Yoshinaga, R. Horiuchi, Trans. Jpn. Inst. Met. 4 (1963) 1–8, doi:10.2320/matertrans1960.4.1.
[15] B. Li, P.F. Yan, M.L. Sui, E. Ma, Acta Mater. 58 (2010) 173–179, doi:10.1016/j.actamat.2009.08.066.
[16] W.B. Hutchinson, M.R. Barnett, Scr. Mater. 63 (2010) 737–740, doi:10.1016/j.scriptamat.2010.05.047.
[17] H. Tonda, S. Ando, Metall. Mater. Trans. A 33 (2002) 831–836, doi:10.1007/s11661-002-0152-z.
[18] S.H. Choi, D.W. Kim, B.S. Seong, A.D. Rollett, Int. J. Plast. 27 (2011) 1702–1720, doi:10.1016/j.ijplas.2011.05.014.
[19] S. Groh, E.B. Marin, M.F. Horstemeyer, D.J. Bammann, Model. Simul. Mater. Sci. Eng. 17 (2009) 075009, doi:10.1088/0965-0393/17/7/075009.
[20] M. Liao, B. Li, M.F. Horstemeyer, Comput. Mater. Sci. 79 (2013) 534–539, doi:10.1016/j.commatsci.2013.07.016.
[21] H. Fan, J.A. El-Awady, J. Appl. Mech. 82 (2015), doi:10.1115/1.4030930.
[22] H. Fan, J.A. El-Awady, Mater. Sci. Eng. A 644 (2015) 318–324, doi:10.1016/j.msea.2015.07.080.
[23] T. Kitahara, S. Ando, M. Tsushida, H. Kitahara, H. Tonda, Key Eng. Mater. 345–346 (2007) 129–132, doi:10.4028/www.scientific.net/KEM.345-346.129.
[24] S. Aubry, M. Rhee, G. Hommes, V.V. Bulatov, A. Arsenlis, J. Mech. Phys. Solids 94 (2016) 105–126, doi:10.1016/j.jmps.2016.04.019.
[25] F.F. Lavrentev, Yu.A. Pokhil, Mater. Sci. Eng. 18 (1975) 261–270, doi:10.1016/0025-5416(75)90179-2.
[26] E. Lilleodden, Scr. Mater. 62 (2010) 532–535, doi:10.1016/j.scriptamat.2009.12.048.
[27] B. Bhattacharya, Plastic Deformation Behavior Of Pure Magnesium In The Temperature Range 4.2K-300K, McMaster University, 2006.
[28] B. Bhattacharya, M. Niewczas, Philos. Mag. 91 (2011) 2227–2247, doi:10.1080/14786435.2011.555783.
[29] B. Li, E. Ma, Philos. Mag. 89 (2009) 1223–1235, doi:10.1080/14786430902936707.
[30] M. Ghazisaeidi, L.G. Hector, W.A. Curtin, Scr. Mater. 75 (2014) 42–45, doi:10.1016/j.scriptamat.2013.11.013.
[31] Z. Wu, W.A. Curtin, Nature 526 (2015) 62–67, doi:10.1038/nature15364.
[32] Z. Wu, W.A. Curtin, Scr. Mater. 116 (2016) 104–107, doi:10.1016/j.scriptamat.2016.01.041.
[33] H. Numakura, Y. Minonishi, M. Koiwa, Philos. Mag. A 62 (1990) 525–543, doi:10.1080/01418619008244917.
[34] H. Numakura, Y. Minonishi, M. Koiwa, Philos. Mag. A 62 (1990) 545–556, doi:10.1080/01418619008244918.
[35] Y. Minonishi, S. Ishioka, M. Koiwa, S. Morozumi, Philos. Mag. A 46 (1982) 761–770, doi:10.1080/01418618208236929.
[36] Y. Minonishi, S. Ishioka, M. Koiwa, S. Morozumi, M. Yamaguchi, Philos. Mag. A 44 (1981) 1225–1237, doi:10.1080/01418618108235805.
[37] D.J. Bacon, M.H. Liang, Philos. Mag. A 53 (1986) 163–179, doi:10.1080/01418618608242819.
[38] M.H. Liang, D.J. Bacon, Philos. Mag. A 53 (1986) 181–204, doi:10.1080/01418618608242820.

[39] M.H. Liang, D.J. Bacon, Philos. Mag. A 53 (1986) 205–220, doi:10.1080/01418618608242821.
[40] J.R. Morris, J. Scharff, K.M. Ho, D.E. Turner, Y.Y. Ye, M.H. Yoo, Philos. Mag. A 76 (1997) 1065–1077, doi:10.1080/01418619708200015.
[41] Y. Tang, J.A. El-Awady, Acta Mater. 71 (2014) 319–332, doi:10.1016/j.actamat.2014.03.022.
[42] K. Srivastava, S.I. Rao, J.A. El-Awady, Acta Mater. 161 (2018) 182–193, doi:10.1016/j.actamat.2018.09.010.
[43] M.H. Yoo, Metall. Trans. A 12 (1981) 409–418, doi:10.1007/BF02648537.
[44] S.R. Agnew, D.W. Brown, C.N. Tomé, Acta Mater. 54 (2006) 4841–4852, doi:10.1016/j.actamat.2006.06.020.
[45] S. Sandlöbes, M. Friák, S. Zaefferer, A. Dick, S. Yi, D. Letzig, Z. Pei, L.F. Zhu, J. Neugebauer, D. Raabe, Acta Mater. 60 (2012) 3011–3021, doi:10.1016/j.actamat.2012.02.006.
[46] S. Sandlöbes, Z. Pei, M. Friák, L.F. Zhu, F. Wang, S. Zaefferer, D. Raabe, J. Neugebauer, Acta Mater. 70 (2014) 92–104, doi:10.1016/j.actamat.2014.02.011.
[47] S.R. Agnew, L. Capolungo, C.A. Calhoun, Acta Mater. 82 (2015) 255–265, doi:10.1016/j.actamat.2014.07.056.
[48] M.R. Barnett, Mater. Sci. Eng. A 464 (2007) 1–7, doi:10.1016/j.msea.2006.12.037.
[49] Q. Yu, L. Qi, R.K. Mishra, J. Li, A.M. Minor, Proc. Natl. Acad. Sci. 110 (2013) 13289–13293, doi:10.1073/pnas.1306371110.
[50] X.Y. Lou, M. Li, R.K. Boger, S.R. Agnew, R.H. Wagoner, Int. J. Plast. 23 (2007) 44–86, doi:10.1016/j.ijplas.2006.03.005.
[51] D. Ando, J. Koike, Y. Sutou, Acta Mater. 58 (2010) 4316–4324, doi:10.1016/j.actamat.2010.03.044.
[52] B.C. Wonsiewicz, Plasticity of Magnesium Crystals, 1966.
[53] R. Ahmad, Z. Wu, W.A. Curtin, Acta Mater. 183 (2020) 228–241, doi:10.1016/j.actamat.2019.10.053.
[54] F. Kang, Z. Li, J.T. Wang, P. Cheng, H.Y. Wu, J. Mater. Sci. 47 (2012) 7854–7859, doi:10.1007/s10853-012-6344-z.
[55] B.Y. Liu, F. Liu, N. Yang, X.B. Zhai, L. Zhang, Y. Yang, B. Li, J. Li, E. Ma, J.F. Nie, Z.W. Shan, Science 365 (2019) 73–75, doi:10.1126/science.aaw2843.
[56] M.I. Baskes, Phys. Rev. B. 46 (1992) 2727–2742, doi:10.1103/PhysRevB.46.2727.
[57] M.I. Baskes, R.A. Johnson, Model. Simul. Mater. Sci. Eng. 2 (1994) 147, doi:10.1088/0965-0393/2/1/011.
[58] Z. Wu, M.F. Francis, W.A. Curtin, Model. Simul. Mater. Sci. Eng. 23 (2015) 015004, doi:10.1088/0965-0393/23/1/015004.
[59] P. Hirel, Comput. Phys. Commun. 197 (2015) 212–219, doi:10.1016/j.cpc.2015.07.012.
[60] J.D. Eshelby, W.T. Read, W. Shockley, Acta Metall. 1 (1953) 251–259, doi:10.1016/0001-6160(53)90099-6.
[61] A.J.E. Foreman, Acta Metall. 3 (1955) 322–330, doi:10.1016/0001-6160(55)90036-5.
[62] C.S. Hartley, Y. Mishin, Acta Mater. 53 (2005) 1313–1321, doi:10.1016/j.actamat.2004.11.027.
[63] S. Plimpton, J. Comput. Phys. 117 (1995) 1–19, doi:10.1006/jcph.1995.1039.
[64] S. Nosé, J. Chem. Phys. 81 (1984) 511–519, doi:10.1063/1.447334.
[65] W.G. Hoover, Phys. Rev. A. 31 (1985) 1695–1697, doi:10.1103/PhysRevA.31.1695.
[66] A. Stukowski, Model. Simul. Mater. Sci. Eng. 18 (2009) 015012, doi:10.1088/0965-0393/18/1/015012.
[67] J.Dana. Honeycutt, H.C. Andersen, J. Phys. Chem. 91 (1987) 4950–4963, doi:10.1021/j100303a014.
[68] J.F. Nye, Acta Metall. 1 (1953) 153–162, doi:10.1016/0001-6160(53)90054-6.
[69] H. Fan, Q. Wang, X. Tian, J.A. El-Awady, Scr. Mater. 127 (2017) 68–71, doi:10.1016/j.scriptamat.2016.09.002.
[70] X. Liu, J.B. Adams, F. Ercolessi, J.A. Moriarty, Model. Simul. Mater. Sci. Eng. 4 (1996) 293, doi:10.1088/0965-0393/4/3/004.
[71] J. Towns, T. Cockerill, M. Dahan, I. Foster, K. Gaither, A. Grimshaw, V. Hazlewood, S. Lathrop, D. Lifka, G.D. Peterson, R. Roskies, J.R. Scott, N. Wilkins-Diehr, Comput. Sci. Eng. 16 (2014) 62–74, doi:10.1109/MCSE.2014.80.